KSCE Journal of Civil Engineering (2016) 20(6):2235-2242
DOI 10.1007/s12205-015-0646-z

Geotechnical Engineering
pISSN 1226-7988, eISSN 1976-3808
www.springer.com/12205

Analysis on Slope Stability Considering Seepage Effect on Effective Stress

Yuanzhan Wang*, Xufei Liu, Zhikai Zhang***, and Panbo Yang******

Received October 28, 2014/Accepted September 13, 2015/Published Online October 28, 2015

Abstract

Interaction between seepage field and soil stress field influences soil effective stress in general consideration. In addition, water erosion in soil skeleton can also affect soil effective stress. The current studies conducted triaxial compression experiments with seepage, Duncan-Chang model analysis, ABAQUS numerical simulation and followed by a case study analysis. Experiments show that the water erosion in soil skeleton reduces effective stress strength of soil, which is quantitatively described by the reduction of equivalent confining pressure. Through analyzing the characteristics of soil stress-strain curves, the equivalent confining pressure is applied to improve Duncan-Chang model. Using the modified Duncan-Chang model as well as considering the interaction between seepage field and soil stress field, ABAQUS software package is employed to simulate triaxial compression experiments with seepage. This method is validated by comparing simulation and experimental results. Furthermore, this method is applied in the case study of the overall stability of bank slope under seepage effect and finds that the modified model is more conservative on safety assessment of slope stability. The studies provided evidences to prove the importance of considering soil skeleton eroded by water flow in slope stability analysis quantitatively and proposed a modified Duncan-Chang model for engineering application with consideration of seepage effect.

Keywords: *seepage, triaxial test, effective stress, equivalent confining pressure, slope stability*

1. Introduction

The bank slopes of rivers and dams are typically influenced by the actions of water flow. The change in water levels can induce seepage in the slope, which may result in the reduction of slope stability and even landslides.

The salient issues of slope instability induced by seepage have attracted international attention from scientists and engineers. Owoputi and Stolte (2001), Chu-Agor *et al.* (2009), Lindow et al. (2009) and Nardi *et al.* (2012) used tank physical model experiments to characterize the erosion damage caused by seepage. Timpong *et al.* (2007) and Li *et al.* (2009) applied centrifuge physical model experiments to study the mechanisms of slope damage brought about by changing water levels. Though these studies did provide direct insight in terms of results, they did not able to comprehensively simulate full-scale environmental phenomena. Using soil test results as a basis, numerical simulation is a viable avenue for stability analysis of slope.

The reliability of numerical simulation results is largely determined by the accuracy of the utilized geo-mechanical soil characteristics. In numerical simulations, the effective stress indexes were typically selected as the base (Gao *et al*., 2004; Lu *et al*., 2007; Berilgen, 2007; Zhang and Dai, 2010; Sun *et al.*, 2012; Ozer and Bromwell, 2012; Regmi *et al*., 2013). However, the changing effective stress affected by seepage erosion was not considered.

Using experimental methodologies, Liu and Zhao (2000) confirmed that besides the mechanical effect of seepage on soil, it also affected the geo-mechanical properties of the soil, which induced displacement and movement among soil particles i.e. the damage effect on soil effective stress intensity. Chang and Zhang (2011) and Sail *et al*. (2011) believes that migration of particles under seepage flow, i.e. suffusion, affects the hydraulic and mechanical behavior of the soil, and experiment measures were developed to investigate the effect of suffusion on soil stress-strain behavior.

In this study, triaxial compression experiments with seepage were carried out to profile undisturbed clay under the effect of seepage. Through analyzing the effective stress characteristics and referencing the equivalent confining pressure from reinforced soil (Yang, 1972), this study quantitatively characterized the

*Professor, State Key Laboratory of Hydraulic Engineering Simulation and Safety, Tianjin Key Laboratory of Harbor and Ocean Engineering, Tianjin University, Tianjin 300072, China (E-mail: yzwang@tju.edu.cn)
**Ph.D. Student, State Key Laboratory of Hydraulic Engineering Simulation and Safety, Tianjin Key Laboratory of Harbor and Ocean Engineering, Tianjin University, Tianjin 300072, China (Corresponding Author, E-mail: xufeiliu@tju.edu.cn)
***Assistant Engineer, CCCC-FHDI Engineering Co., Ltd., Guangzhou 510230, China (E-mail: zkzhang@tju.edu.cn)
****Master Student, State Key Laboratory of Hydraulic Engineering Simulation and Safety, Tianjin Key Laboratory of Harbor and Ocean Engineering, Tianjin University, Tianjin 300072, China (E-mail: ypb890529@163.com)

damage effect of seepage in soil skeleton, utilizing the reduction of equivalent confining pressure. Through analyzing the characteristics of soil stress-strain curve, the equivalent confining pressure was applied to Duncan-Chang model (Duncan and Chang, 1970). On the basis of modified Duncan-Chang model, this study utilized finite element package, ABAQUS, to simulate the triaxial compression experiments with seepage. This method was validated by comparing simulation and experimental results. Furthermore, this method was applied to the numerical simulation of the entire stability of bank slope under the effect of seepage.

2. Experiment Apparatus and Method

The experiments were carried out with a type SLB-1 stress-strain controlled triaxial shear seepage test apparatus, as shown in Fig. 1. The diameter of sample was 3.91 cm, and the height was 8 cm.

① Isotropic consolidation was applied to the soil sample after vacuum pumping saturation. Consolidation was performed when the pore pressure dissipated to zero. ② The seepage pressure was applied upward to soil sample from the bottom to ensure that the seepage path was across all the sample. ③ When the top of the soil sample attained a stable rate of overflowed water, it indicated the seepage in soil reached a steady state. At this time, stain controlled shear process was used to shear the soil sample at constant rate of 0.1 mm/min until the axial strain of soil sample reached 15%. The soil sample was then considered to be in a damaged state.

3. Experiment Results

The samples were taken from the upstream of Youjiang River in Naji area, Guangxi. The sample was determined to be clay, and had a natural density of 2.240 g/cm^3 and a dry density of 1.772 g/cm^3; the natural moisture content was 26.39% and its specific weight was 2.729.

To coordinate with the actual depth where the soil samples were collected, the experimental confining pressures were set to 20 kPa, 27 kPa and 35 kPa. The hydraulic gradients were set to 0, 5, 7.5 and 12.5, and were set up by back pressure control. The back pressure at the top was set to zero and the back pressure at the bottom was set to the value calculated by the hydraulic gradient and specimen size.

Table 1. Effective Shear Strength Indexes of the Soil

Hydraulic gradient i	Effective angle of internal friction φ' (°)	Effective cohesion c' (kPa)
0	22.08	9.34
5	22.19	6.67
7.5	22.02	5.24
12.5	22.08	2.94

The effective shear strength indexes of the soil were obtained from the experimental results, as shown in Table 1.

4. Modified Duncan-Chang model with Considering Seepage Effect

4.1 Concept of Equivalent Confining Pressure

Indicated in the experiment results shown in Table 1, as the hydraulic gradient increasing, the effective angle of internal friction, φ', is almost invariant, while the effective cohesion, c', is decreasing. Under the assumption that seepage does not influence the effective angle of internal friction, seepage influence on soil drainage shear characteristics is derived according to Mohr-Coulomb criterion.

The effective stress Mohr circle under the influence of seepage is shown in Fig. 2. In the figure, φ' is the effective angle of internal friction of the soil, c' is the effective cohesion of the soil without seepage, c_s' is the effective cohesion of the soil with seepage, $(\sigma_1-\sigma_3)$ is the diameter of the stress circle under the confining pressure of σ_3 without seepage, $(\sigma_{1s}-\sigma_3)$ is the diameter of the stress circle under the confining pressure of σ_3 with seepage, $(\sigma_{1s}-\sigma_{3s})$ is the diameter of the stress circle under the confining pressure of σ_{3s} without seepage.

When the soil with seepage under the confining pressure of σ_3 is in limit equilibrium state (corresponding to the stress circle of σ_3~σ_{1s}), σ_{1s} is shown as Eq. (1).

$$\sigma_{1s} = \sigma_3 \tan^2\left(45^\circ + \frac{\varphi'}{2}\right) + 2c_s' \tan\left(45^\circ + \frac{\varphi'}{2}\right) \quad (1)$$

When the soil without seepage reaches the limit equilibrium state as σ_{1s}, the required confining pressure is σ_{3s} (corresponding to the stress circle of σ_{3s}~σ_{1s}). σ_{1s} is shown as Eq. (2).

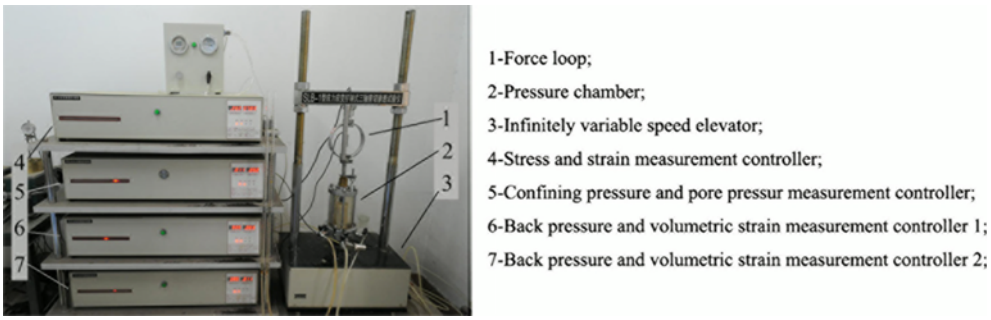

Fig. 1. Type SLB-1 Stress-strain Controlled Triaxial Shear Seepage Test Apparatus

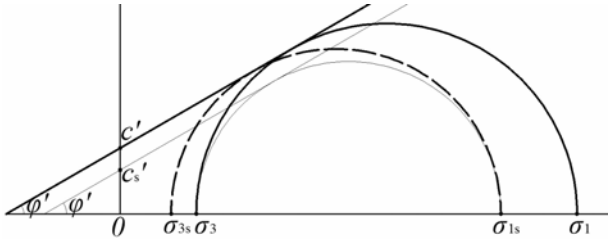

Fig. 2. Effective Stress Mohr Circle of the Soil

$$\sigma_{1s} = \sigma_{3s}\tan^2\left(45^\circ+\frac{\varphi'}{2}\right)+2c'\tan\left(45^\circ+\frac{\varphi'}{2}\right) \quad (2)$$

Combining Eq. (1) and Eq. (2), (c'–c_s') is derived out, as shown in Eq. (3).

$$c'-c_s' = \frac{\sigma_3-\sigma_{3s}}{2}\tan\left(45^\circ+\frac{\varphi'}{2}\right) \quad (3)$$

When the soil without seepage with the confining pressure of σ_3 is in limit equilibrium state (corresponding to the stress circle of σ_3~σ_1), σ_1 is shown as Eq. (4).

$$\sigma_1 = \sigma_3\tan^2\left(45^\circ+\frac{\varphi'}{2}\right)+2c'\tan\left(45^\circ+\frac{\varphi'}{2}\right) \quad (4)$$

Subtracting Eq. (2) from Eq. (4), (σ_3–σ_{3s}) is derived out, as shown in Eq. (5).

$$\sigma_3-\sigma_{3s} = (\sigma_1-\sigma_{1s})\tan^2\left(45^\circ-\frac{\varphi'}{2}\right) \quad (5)$$

Substituting Eq. (5) into Eq. (3), ($c'-c_s'$) is derived out, as shown in Eq. (6).

$$c'-c_s' = \frac{\sigma_1-\sigma_{1s}}{2}\tan\left(45^\circ-\frac{\varphi'}{2}\right) \quad (6)$$

Under the assumption that seepage does not affect soil's effective angle of internal friction, the decreased value of effective cohesion under seepage conditions, (c'–c_s'), can be calculated according to Eq. (6). The calculated value is compared with the experimental data from Table 1, as show in Table 2.

The discrepancy between the calculated and experimental values in Table 2 is relatively small, indicating that the effect of seepage on effective shear strength indexes can be explained by the consistency of effective angle of internal friction and decreasing cohesion.

(σ_3–σ_{3s}) is the reduction value of the equivalent confining pressure, which is used to describe the influence of a certain hydraulic gradient on the effective stress of the soil, and reflects the damage of water flow in soil skeleton during the seepage process. σ_{3s} is defined as the equivalent confining pressure, meaning that the soil under the confining pressure of σ_{3s} without seepage reaches the same limit equilibrium state of stress with that under the confining pressure of σ_3 with seepage.

Combing experimental results and Eq. (5), one can calculate (σ_3–σ_{3s}) under different confining pressures and seepage working conditions, as shown in Table 3.

Table 2. Comparison between the Calculated Value and Experimental Data for the Effect of Seepage on Soil's Effective Cohesion

Hydraulic gradient i	Calculated value of (c'–c_s') (kPa)	Experimental data of (c'–c_s') (kPa)	Error
5	2.581	2.673	-3.43%
7.5	4.152	4.103	1.21%
12.5	6.397	6.398	-0.02%

Table 3. Reduction of Equivalent Confining Pressure under Different Seepage Working Conditions

Hydraulic gradient i	Confining pressure σ_3 (kPa)	(σ_3–σ_{3s}) (kPa)	Averaged (σ_3–σ_{3s}) (kPa)
5	20	3.627	3.476
	27	3.174	
	35	3.627	
7.5	20	5.441	5.592
	27	5.894	
	35	5.441	
12.5	20	8.614	8.614
	27	8.614	
	35	8.614	

In Table 3, it is shown that the reduction value of equivalent confining pressure (σ_3–σ_{3s}) is only correlated with hydraulic gradient i, not with the confining pressure. Eq. (7) can be fitted to describe the relationship between the reduction value of confining pressure and hydraulic gradient i.

$$\sigma_3-\sigma_{3s} = 0.7031i \quad (7)$$

4.2 Initial Tangent Modulus with Considering Seepage Effect

According to Kondner's study (Kondner, 1963), the relationship between stress and strain in triaxial tests is approximately hyperbolic, as shown in Eq. (8).

$$q = \frac{\varepsilon_a}{a+b\varepsilon_a} \quad (8)$$

where ε_a is axial strain (%), q is the deviator stress (kPa), a is the inverse of the initial tangent modulus E_i, and b is the inverse of asymptote of stress-strain curve.

The solid points in Figs. 3, 4 and 5 are experimental data, and the solid line is obtained by fitting experimental data according to Eq. (8). It can be seen from the contrast between experimental data and solid line that the hyperbolic relationship is fit to the experimental data.

According to Janbu's study about compression tests (Janbu, 1963), the relationship between the initial tangent modules E_i and the confining pressure σ_3 can be written as Eq. (9).

$$E_i = Kp_a\left(\frac{\sigma_3}{p_a}\right)^n \quad (9)$$

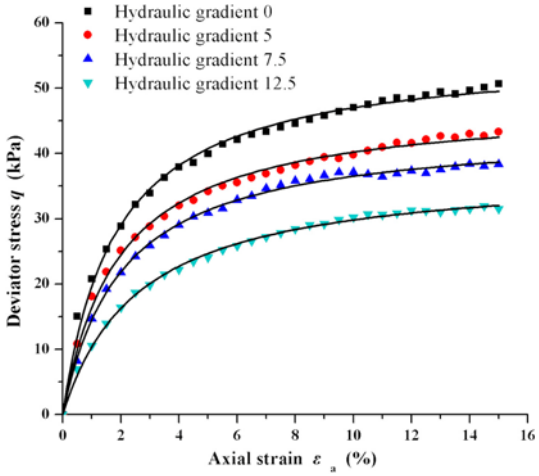

Fig. 3. Hyperbolic Fitting of the Stress-strain Curve with Confining Pressure of 20 kPa

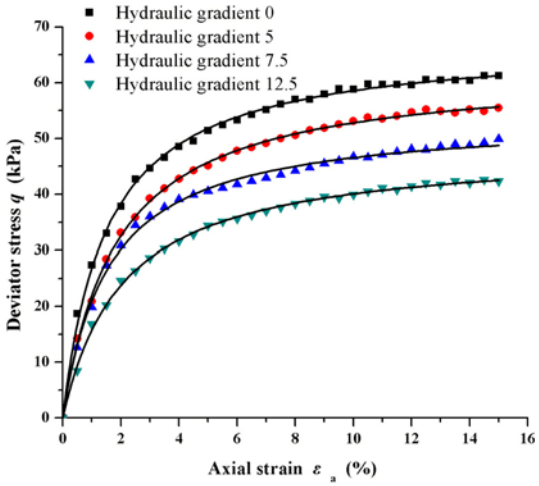

Fig. 4. Hyperbolic Fitting of the Stress-strain Curve with Confining Pressure of 27 kPa

Where K and n are the experimentally determined coefficients and p_a is atmospheric pressure.

Transforming Eq. (9), the relationship between E_i and σ_3 can also be written as Eq. (10).

$$\lg E_i = \lg(Kp_a) + n\lg\frac{\sigma_3}{p_a} \tag{10}$$

Equation (10) indicates that $\lg E_i$ has a linear relationship with $\lg(\sigma_3/p_a)$. By replacing σ_3 in Eq. (10) with σ_{3s} in Eq. (5), we calculated $\lg E_i$ and $\lg(\sigma_{3s}/p_a)$ for different working conditions, respectively. The fitted curve is shown in Fig. 6.

From Fig. 6, it can be seen that $\lg E_i$ and $\lg(\sigma_{3s}/p_a)$ display a linear relationship, and the fitted equation is shown in Eq. (11).

$$\lg E_i = 4.32687 + 1.210711g\frac{\sigma_{3s}}{p_a} \tag{11}$$

i.e.,

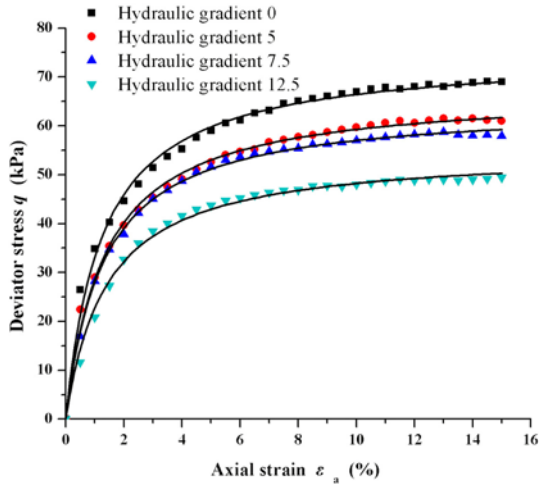

Fig. 5. Hyperbolic Fitting of the Stress-strain Curve with Confining Pressure of 35 kPa

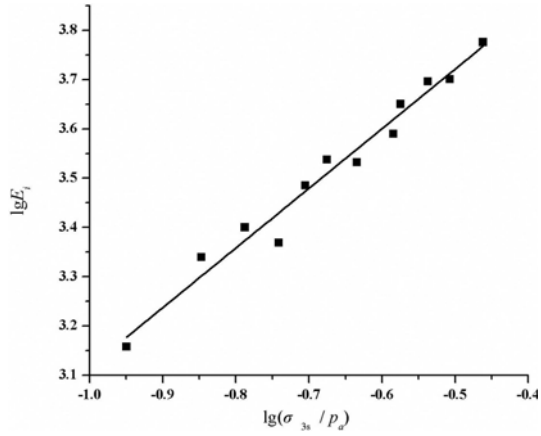

Fig. 6. Fitted Curve between $\lg E_i$ and $\lg(\sigma_{3s}/p_a)$

$$E_i = 209.4749p_a\left(\frac{\sigma_{3s}}{p_a}\right)^{1.21071} \tag{12}$$

4.3 Numerical Simulation of Triaxial Shear Tests with Seepage

The Duncan-Chang model is a non-linear elastic model and the tangent elastic modulus E_t is written as Eq. (13).

$$E_t = \frac{\partial q}{\partial \varepsilon_a} = Kp_a\left(\frac{\sigma_{3s}}{p_a}\right)^n\left(1 - R_f\frac{q}{q_f}\right)^2$$
$$q_f = \frac{2c'\cos\varphi' + 2\sigma_{3s}\sin\varphi'}{1-\sin\varphi'} \tag{13}$$

Where K and n are coefficients determined from Eq. (12), which are 209.4749 and 1.21071, respectively. p_a is atmospheric pressure, 101.33 kPa. R_f is damage ratio, which is set as 0.92 according to experimental results. q_f is the strength when soil damage. φ' is the effective angle of internal friction of the soil without seepage, which is taken from an averaged experimental value, i.e., 22.09°, as shown in Table 1. c' is effective cohesion of the soil without seepage, i.e., 9.34 kPa, according to the

experimental result in Table 1.

The Duncan-Chang model assumes that the axial strain ε_a has a hyperbolic relationship with lateral strain ε_r (Kulhawy *et al*., 1969), as shown in Eq. (14), where the relation between f and confining pressure follows Eq. (15). Therefore, the tangent Poisson ratio at an arbitrary point v_t can be written as Eq. (16).

$$\frac{-\varepsilon_r}{\varepsilon_a} = f - D\varepsilon_r \tag{14}$$

$$f = G - F\lg\left(\frac{\sigma_{3s}}{p_a}\right) \tag{15}$$

$$v_t = -\frac{d\varepsilon_r}{d\varepsilon_a} = \frac{G - F\lg\left(\frac{\sigma_{3s}}{p_a}\right)}{\left(1 - \frac{Dq}{Kp_a\left(\frac{\sigma_{3s}}{p_a}\right)^n\left[1 - R_f\frac{q}{q_f}\right]}\right)} \tag{16}$$

In Eqs. (14) and (15), f, D, G and F are obtained from the relational curve between experimental axial strain ε_a and lateral strain ε_r. Under a confining pressure of 20 kPa, the relational curve between axial strain ε_a and lateral stain ε_r is shown in Fig. 7 (The curves under confining pressures of 27 kPa and 35 kPa show similar results, but are not listed due to the length limitation of this paper). In Fig. 7, $-\varepsilon_r$ and ε_a exhibit a linear relation, thus D is equal to 0. According to the fitting result between $-\varepsilon_r$ and ε_a, the value of f is obtained, as shown in Fig. 8. Fitting results provided: G is 0.3674 and F is 0.0285.

Using the above parameters, the subroutine for modified Duncan-Chang model is programmed. Based on the modified Duncan-Chang model, the commercial finite element software, ABAQUS, is used to simulate triaxial compression experiments with seepage. The height of model is 8 cm and with a diameter of 3.91 cm, and the element type is C3D8P, as shown in Fig. 9.

In the numerical simulation, Function I is the interaction between seepage field and soil stress field. Function II is the damage effect of seepage in soil skeleton which is represented by the corresponding equivalent confining pressure σ_{3s}.

In Figs. 10, 11 and 12, the lines with solid points are experimental data and the lines with empty points are simulation results with consideration of effects of Function I and II. In Figs. 13, 14 and 15, the lines with solid points are same with those in Figs. 10, 11 and 12, while the lines with empty points are simulation results with solitary consideration of Function I.

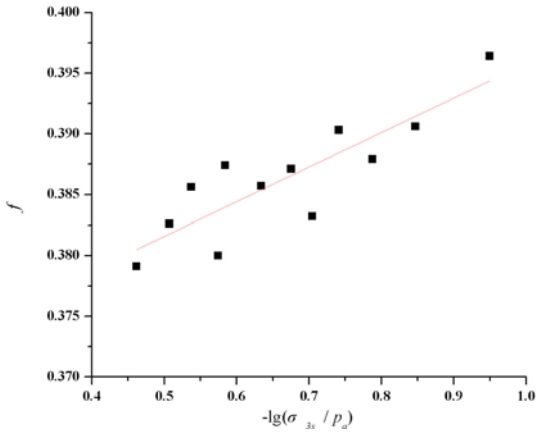

Fig. 8. Relation between f and -lg(σ_{3s}/p_a) at Different Working Conditions

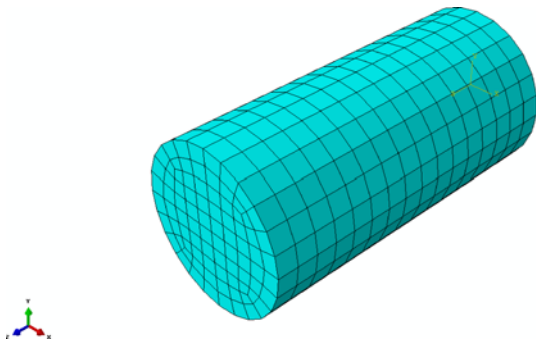

Fig. 9. Finite Element Model of Triaxial Compression Tests with Seepage

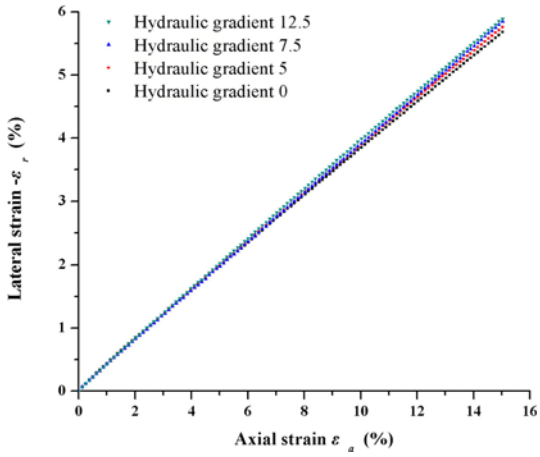

Fig. 7. Relational Curve between Axial Strain ε_a and Lateral Strain ε_r under a Confining Pressure of 20 kPa

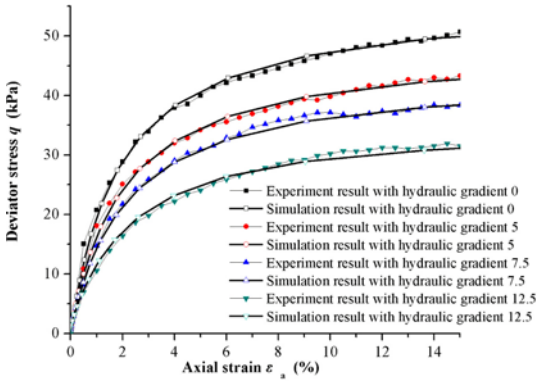

Fig. 10. Comparisons between Simulation Results (Function I and II) and Experiment Results under a Confining Pressure of 20 kPa

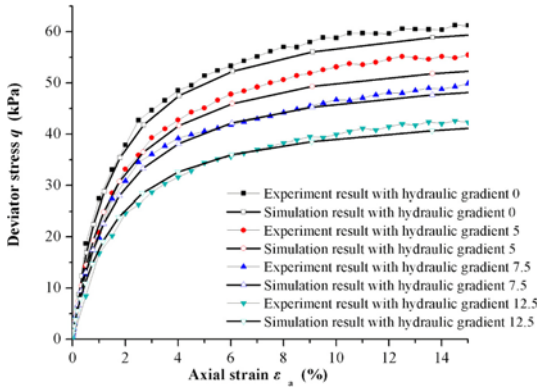

Fig. 11. Comparisons between Simulation Results (Function I and II) and Experiment Results under a Confining Pressure of 27 kPa

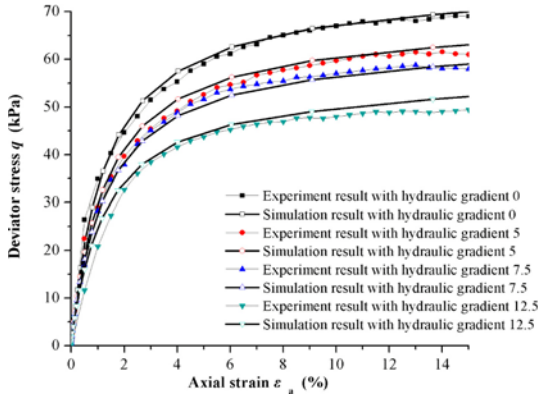

Fig. 12. Comparisons between Simulation Results (Function I and II) and Experiment Results under a Confining Pressure of 35 kPa

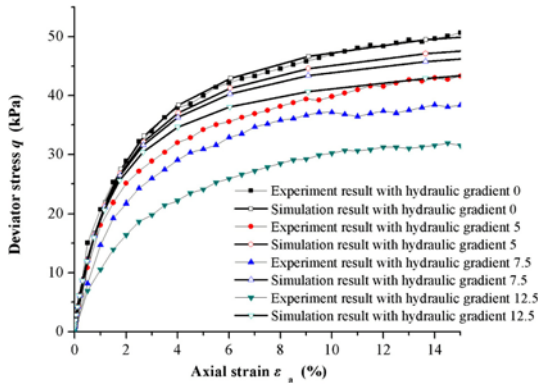

Fig. 13. Comparisons between Simulation Results (Function I) and Experiment Results under a Confining Pressure of 20 kPa

Comparing Figs. 10, 11, 12 and Figs. 13, 14, 15, it can be seen that the simulation result using modified Duncan-Chang model are fitting better with experiment results than those of nonuse.

5. An Engineering Case for Bank Slope Stability Analysis

Based on the modified Duncan-Chang model, this study

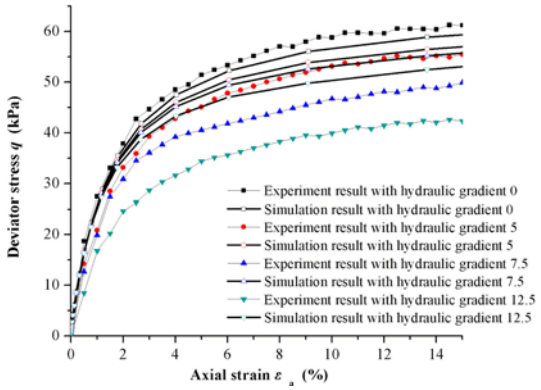

Fig. 14. Comparisons between Simulation Results (Function I) and Experiment Results under a Confining Pressure of 27 kPa

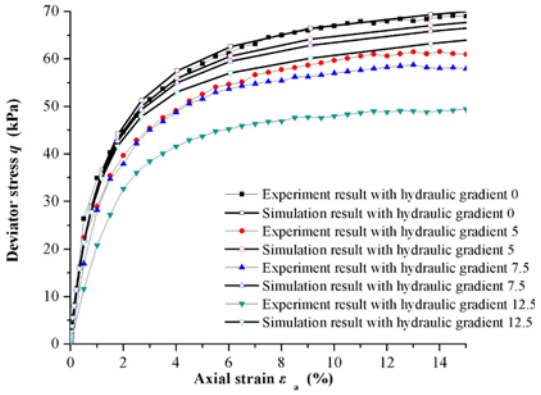

Fig. 15. Comparisons between Simulation Results (Function I) and Experiment Results under a Confining Pressure of 35 kPa

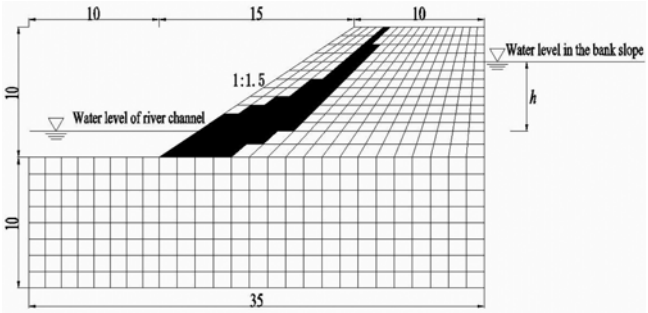

Fig. 16. Sketch of Numerical analysis for Slope Stability

performed overall stability analyses for soil bank slopes undergoing seepage in the soil. As this issue is a plane strain problem, the established model is two-dimensional using CPE4P as the element type, and 460 elements with 509 nodal points, as shown in Fig. 16. The water depth in the river channel is 2 m. Seepage happens outwardly from the inside slope. The water depth difference between the left and right boundaries, h, is used to describe the seepage intensity.

In the finite element calculation, the turning point in the curve which is the energy of critical sliding zone changing with reduction factor is used for instability criterion (Shi *et al*., 2013). The critical sliding zone is shown as the shaded area in Fig. 16.

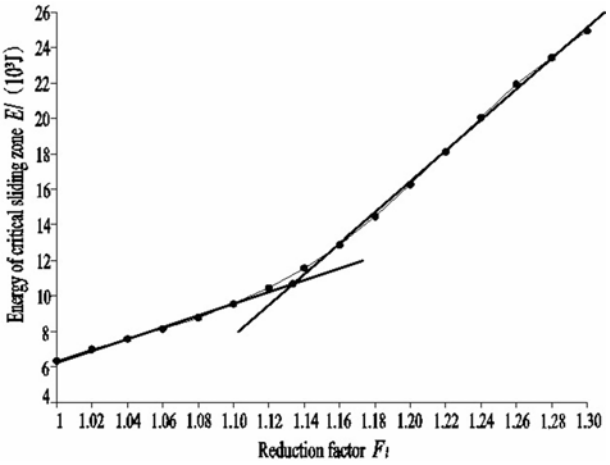

Fig. 17. Variation Curve of Critical Sliding Zone Energy *E*, with Respect to the Reduction Factor, *F*

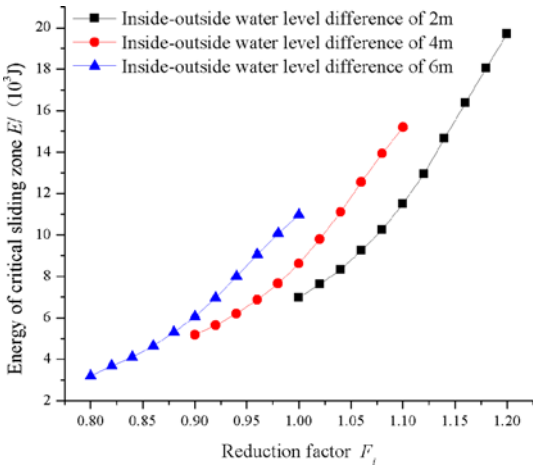

Fig. 18. Relational Curves of Critical Sliding Zone Energy *E* and Reduction Factor F_i (Function I)

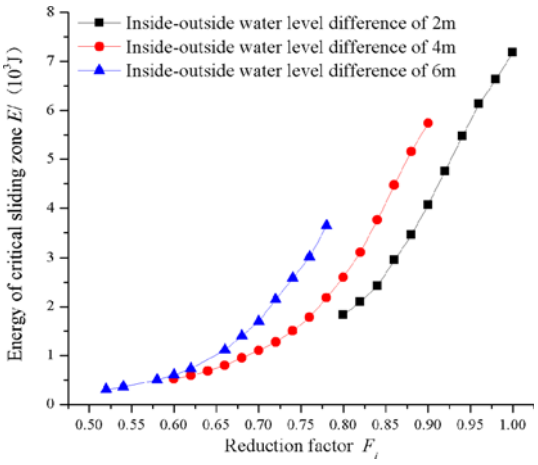

Fig. 19. Relational Curves of Critical Sliding Zone Energy *E* and Reduction Factor F_i (Function I and II)

The energy of critical sliding zone can be simplified as the summation of the elements' deformation energy where the arc passes, *E*. The curve of variation of total energy *E* with respect to the reduction factor F_i is plotted in Fig. 17. This curve can be treated as two linear functions: with increase of reduction factor, the energy of sliding zone increases in a near linear fashion; when a critical point reaches, the increase of sliding zone energy accelerates with increase of reduction factor. The intercept of these two lines can be considered as the critical damage point of the slope, and the corresponding reduction factor is the safety factor.

When there is no seepage in the bank slope, the Duncan-Chang model and Morgenstern-Price slices method are severally used to calculate the safety factor of the overall stability, as shown in Table 4.

In Table 4, it can be seen that the safety factor calculated by using Duncan-Chang model is only 2% higher than that generated by Morgenstern-Price slice method, which indicates the reliability of Duncan-Chang model for the calculation of the safety factor of bank slope stability.

When seepage happens in the bank slope, the safety factors of the bank slope in sole consideration of Function I, and consideration of both Function I and II are shown in Table 5. Fig. 18 is the relationship curves between the corresponding sliding zone energy *E* and reduction factor F_i of the former, and Fig. 19 is the relationship curves of the latter.

As shown in Table 5, the modified model is more conservative on safety assessment of slope stability. For safety purposes, the seepage failure in soil skeleton should be an essential consideration while calculating the slope stability.

Table 4. Safety Factor of Overall Stability oF Bank Slope Without Seepage

Method	Duncan-Chang model	Morgenstern-Price slice method
Safety factor	1.134	1.111

Table 5. Safety Factor of Bank Slope Undergoing Seepage

Inside and outside water level difference of bank slope *h* (m)	Function I	Function I and II
2	1.089	0.848
4	0.983	0.770
6	0.867	0.654

6. Conclusions

Implementation of triaxial compression tests, modification of Duncan-Chang model, ABAQUS simulation and a case study analysis of modified Duncan-Change model are demonstrated with focus of seepage failure. The conclusions are drawn as follows.

1. The effect of seepage failure on soil effective stress indexes are characterized by no variation of the angle of internal friction and a decreasing cohesion . Furthermore, based on the concepts of equivalent confining pressure deduced from the

Mohr-Coulomb criterion, this study proposes to use the reduction of equivalent confining pressure to quantify the seepage damage effect in soil skeleton.

2. Through analysis of soil stress-strain curve, this study applies the equivalent confining pressure to Duncan-Chang model, and proposes a modified Duncan-Chang model with the consideration of seepage effect.
3. On the basis of modified Duncan-Chang model incorporating the interaction between seepage field and soil stress field, the finite element software, ABAQUS, is used to simulate triaxial compression tests with seepage. Through comparisons between the numerical simulations and experimental results, the modified Duncan-Chang model is validated.
4. The modified Duncan-Chang model is further applied to numerically simulate the overall slope stability with seepage in Youjiang River and finds that the modified model is more conservative on safety assessment of slope stability.

Acknowledgements

The research work is sponsored by the National Natural Science Foundation of China (51279128).

References

Berilgen, M. M. (2007). "Investigation of stability of slopes under drawdown conditions." *Computers and Geotechnics*, Vol. 34, No. 2, pp. 81-91, DOI: 10.1016/j.compgeo.2006.10.004.

Chang, D. S. and Zhang, L. M. (2011). "A stress-controlled erosion apparatus for studying internal erosion in soils." *Geotechnical Testing Journal*, Vol. 34, No. 6, pp. 579-589.

Chu-Agor, M. L., Fox, G. A., and Wilson, G. V. (2009). "Empirical sediment transport function predicting seepage erosion undercutting for cohesive bank failure prediction." *Journal of Hydrology*, Vol. 377, Nos. 1-2, pp. 155-164, DOI: 10.1016/j.jhydrol.2009.08.020.

Duncan, J. M. and Chang, C. Y. (1970). "Nonlinear analysis of stress and strain in soils." *Journal of the Soil Mechanics and Foundation Division*, Vol. 96, No. SM5, pp. 1629-1653.

Gao Xiaoyu, Liao Hongjian, and Ding Chunhua (2004). "Seepage effects on soil slope stability." *Rock and Soil Mechanics*, Vol. 25, No. 1, pp. 69-72, DOI: 0.3969/j.issn.1000-7598.2004.01.014. (In Chinese)

Janbu, N. (1963). *Soil compressibility as determined by oedometer and triaxial tests*, In Proceedings of the 3rd European Conference on Soil Mechanics and Foundation Engineering, Wiesbaden, Germany, pp. 19-25.

Kondner, R. L. (1963). "Hyperbolic stress-strain response: Cohesive soils." *Journal of Soil Mechanics and Foundations, American Society of Civil Engineers*, Vol. 89, No. SM1, pp. 115-143.

Kulhawy, F. H., Duncan, J. M., and Seed, H. B. (1969). "Finite element analyses of stresses and movements in embankments during construction." *Geotechnical Engineering Report,* No. TE 69-4, Berkeley, University of California.

Li Shaojun, Knappett, J., and Feng, Xiating (2009). *Investigation of slope stability influenced by change of reservoir water level in Three Gorges of China,* International Forum on Porous Flow and Applications, Wuhan, China, pp. 911-916.

Lindow, N., Fox, G. A., and Evans, R. O. (2009). "Seepage erosion in layered stream bank material." *Earth Surface Processes and Landforms*, Vol. 34, No. 12, pp. 1693-1701, DOI: 10.1002/esp.1874.

Liu Guangsheng and Zhao Weibing (2000). "Effect of seepage on shear strength of silt soil in foundation excavation." *Journal of Nanjing Hydraulic Research Institute*, No. 1, pp. 54-57, DOI: 10.3969/j.issn.1009-640X.2000.01.009. (In Chinese)

Lu Bo, Ding Xiuli, and Dong Zhihong (2007). "Analysis of the influence of reservoir impoundment on slope stability using strength reduction method based on ABAQUS." *Journal of Sichuan University (Engineering science Edition)*, Vol. 39, No. z1, pp. 96-103. (In Chinese)

Nardi, L., Rinaldi, M., and Solari, L. (2012). "An experimental investigation on mass failures occurring in a riverbank composed of sandy gravel." *Geomorphology*, Vol. 163, pp. 56-69, DOI: 10.1016/j.geomorph.2011.08.006.

Owoputi, L. O. and Stolte, W. J. (2001), "The role of seepage in erodibility." *Hydrological Processes*, Vol. 15, No. 1, pp. 13-22, DOI: 10.1002/hyp.153.

Ozer, A. T. and Bromwell, L. G. (2012). "Stability assessment of an earth dam on silt/clay tailings foundation: A case study." *Engineering Geology*, Vol. 151, pp. 89-99, DOI: 10.1016/j.enggeo.2012.09.011.

Regmi, R. K., Lee, G., and Jung, K. (2013). "Analysis on failure of slope and landslide dam." *KSCE Journal of Civil Engineering*, Vol. 17, No. 5, pp. 1166-1178, DOI: 10.1007/s12205-013-0049-y.

Sail, Y., Marot, D., Sibille, L., and Alexis, A. (2011). "Suffusion tests on cohesionless granular matter Experimental study." *European Journal of Environmental and Civil Engineering*, Vol. 15, No. 5, pp. 799-817, DOI: 10.3166/EJECE.15.799-817.

Shi Jianyong, Cao Qiurong, and Zhou Lufei (2013). "Modified finite element method for shear strength reduction and instability criterion in slope stability analysis." *Rock and Soil Mechanics*, Vol. 34, No. z2, pp. 237-241. (In Chinese)

Sun Xushu, Li Jianlin, Liu Jie, and Luo Rong (2012). "Coupling numerical analysis of seepage and stress fields after excavation of slope." *International Conference on Modern Hydraulic Engineering, Nanjing, China*, Vol. 28, pp. 336-340, DOI: 10.1016/j.proeng.2012. 01.729.

Timpong, S., Itoh, K., and Toyosawa, Y. (2007). "Geotechnical centrifuge modelling of slope failure induced by ground water table change." *International Conference on Landslides and Climate Change, Ventnor, England*, pp. 107-112.

Yang, Z. (1972). *Strength and deformation characteristic of reinforced sand,* Dissertation presented to the University of California, at Los Angeles, California.

Zhang Xiaoyong and Dai Zihang (2010). "Analysis of slope stability under seepage by using ABAQUS program." *Chinese Journal of Rock Mechanics and Engineering*, Vol. 29, No. z1, pp. 2927-2934. (In Chinese)